https://doi.org/10.3311/PPci.22310

Periodica Polytechnica Civil Engineering, 68(3), pp. 925–936, 2024

An Analytical Model for the Initial Stiffness of Bearing Connections with Slotted Holes

Edouard Cavène[1], Évelyne Toussaint[1*], Sébastien Durif[1], Abdelhamid Bouchaïr[1]

[1] Université Clermont Auvergne, CNRS, SIGMA Clermont, Institut Pascal, 2 Avenue Blaise Pascal, F-63000 Clermont-Ferrand, France

[*] Corresponding author, e-mail: evelyne.toussaint@uca.fr

Received: 31 March 2023, Accepted: 02 March 2024, Published online: 13 May 2024

Abstract

In steel structures, cover plate joints are mainly used with normal round holes, but slotted holes, where the slot is oriented perpendicular to the direction of the bearing force, make it possible to release displacements in selected directions and thus better control the complex state of stresses in the connected plates. This study investigates the initial stiffness of a cover plate with a single slotted hole. The aim of this paper is to propose an analytical model that predicts the initial stiffness of slotted holes with respect to experimental results obtained on a panel of different geometries. This approach makes it possible to evaluate the effects of the end distances on the bending of the plate compared to the bearing under the bolt. A large panel of geometries is tested to quantify the experimental value of initial stiffness using Digital Image Correlation (DIC) technique compared to Linear Variable Differential Transformer (LVDT) sensors. To evaluate the initial stiffness, a method of processing experimental data is developed that allows a reproducible determination of stiffnesses. An analytical model is then proposed based on the improvement of existing models available in the literature. It is validated for different specimen geometries considering the contribution to the initial stiffness due to bending, shearing and support of the steel plate under the bolt. The comparisons show that the proposed analytical model can predict the initial stiffness of different geometries of tested specimens with slotted holes.

Keywords

cover-plate joints, slotted hole, initial stiffness, experimental tests, analytical model

1 Introduction

Most of the research activities on steel bolted connections are dedicated to strength analysis to propose analytical design models that allow structural stability and bearing capacity. In this context, numerous studies deal with the analysis of the parameters influencing the failure of steel connections (geometry, material, number of bolts) [1–7] and design models that allow their strength to be predicted [8, 9].

In addition, steel has the ability of large deformation capacity with high level of strength capacity. Therefore, the deformation of the connection under load is a key point to be studied in the current context of semi-rigid connection design. The European design code Eurocode 3 part 1–8 [10] proposes a method to predict the stiffness of the connection based on the stiffness of all its components [11, 12]. The stiffness components involved in bearing type connections are shearing of the bolt and bearing of the plate under bolt load.

The bearing is the main source of deformation and ductility of bolted joints of the bearing type [13]. Design models for the stiffness of normal round holes in bearings that exist in the literature [14] and standards [10] show good prediction of initial stiffness. Slotted holes have some applications under cyclic loading to reduce the stress level on the connected elements and to improve stress distribution as in the connection of hollow structural steel (HSS) beams to concrete filled steel tube (CFST) [15]. However, there is very little research on their bearing stiffness (see for example a model by Wald et al. [16].

The estimation of the initial stiffness is a key point in the characterization of bearing type bolted joints, mainly with oblong holes. The present study is based on a large experimental campaign using Digital Image Correlation (DIC) technique with the aim of proposing a model to predict the initial stiffness for slotted holes. Different hole

Cite this article as: Cavène, E., Toussaint, É., Durif, S., Bouchaïr, A. "An Analytical Model for the Initial Stiffness of Bearing Connections with Slotted Holes", Periodica Polytechnica Civil Engineering, 68(3), pp. 925–936, 2024. https://doi.org/10.3311/PPci.22310

lengths and end distances are tested to cover a realistic variety of slotted holes.

In the first part of this paper, the experimental setup and methods are presented. An analytical model is then developed to predict the initial stiffness of the joints tested. Finally, both qualitative and quantitative analyses are proposed, based on the experimental results, demonstrating the acceptability of the proposed analytical model.

2 Experimental programs

The aim of the experimental program was to quantify the initial stiffness of slotted cover plates in bearing type joints, where the slot is perpendicular to the direction of the bearing force. The geometrical and mechanical characteristics of the specimens tested are presented below. A measurement technique based on DIC is then used to accurately measure the relative displacement between the bolt and the plate.

2.1 Design of specimens

25 steel plates 6 mm thick are tested with five-hole lengths (L_0) and five end distances (e_3) for each hole length. Geometrical characteristics of a slotted hole are presented in Fig. 1. Geometries and number of samples are summarized in Table 1. For each geometry, two or three replications were performed. In total, this campaign includes 59 samples with 25 different geometries (Table 1).

The name of each sample is *Ei-j*: *i* is the multiplication factor of the hole diameter d_0 to obtain the length of the slotted hole L_0 and *j* is the multiplication factor of the hole diameter d_0 to obtain the end distance e_3. For example, sample *E*1-1.5 is characterized by a hole length L_0 equal to 1 d_0 and an end distance e_3 equal to 1.5 d_0.

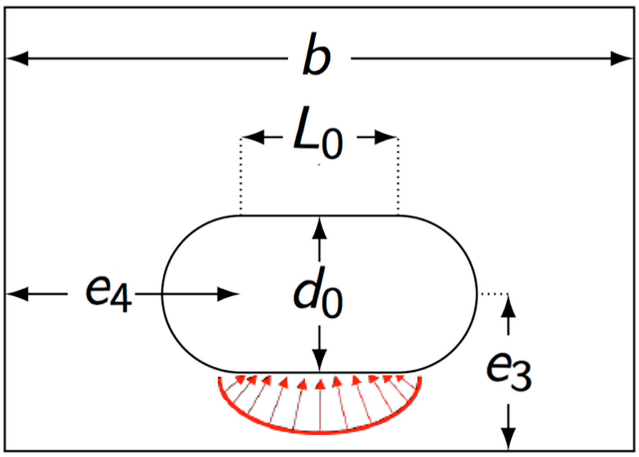

Fig. 1 Geometrical characteristics of a slotted hole: e_3 varies from 13 to 26 mm; e_4 = 26 mm; d_0 = 13 mm; b varies from 65 to 91 mm; L_0 varies from 13 to 39 mm

Table 1 Geometrical characteristics of the tested specimens in mm

Specimen	e_3 (mm)	e_4 (mm)	d_0 (mm)	b (mm)	L_0 (mm)	Number of tests
*E*1-1	13					2
*E*1-1.25	16.25					2
*E*1-1.5	19.5	26	13	65	13	2
*E*1-1.75	22.85					2
*E*1-2	26					2
*E*1.5-1	13					3
*E*1.5-1.25	16.25					3
*E*1.5-1.5	19.5	26	13	71.5	19.5	2
*E*1.5-1.75	22.85					2
*E*1.5-2	26					2
*E*2-1	13					2
*E*2-1.25	16.25					2
*E*2-1.5	19.5	26	13	78	26	2
*E*2-1.75	22.85					2
*E*2-2	26					2
*E*2.5-1	13					3
*E*2.5-1.25	16.25					3
*E*2.5-1.5	19.5	26	13	84.5	32.5	2
*E*2.5-1.75	22.85					3
*E*2.5-2	26					3
*E*3-1	13					3
*E*3-1.25	16.25					2
*E*3-1.5	19.5	26	13	91	39	3
*E*3-1.75	22.85					2
*E*3-2	26					3

2.2 Material properties

The specimens tested were made from S355MC steel with a yield strength of 411.5 MPa and an ultimate strength of 484.8 MPa. These values were obtained from tensile coupon tests. Using a Young's modulus of 210 GPa, the corresponding yield strain is estimated to be 0.19%.

The pin used for the displacement measurements with the LVDT sensors (Fig. 2) is made of maraging steel and has a yield strength of 1998 MPa and an ultimate strength of 2050 MPa. The maximum elongation is about 7%. This material was chosen to avoid the pin yielding in bending, which could cause out-of-plane displacement of the plates during the tensile tests.

2.3 Experimental setup

The tests were carried out on a ±200 kN Zwick testing machine using a symmetrical two-plate setup to avoid rotation of the pin used as a fixture during the tests. Fig. 2 shows the test setup where the load is transferred through two symmetrical plates. One of the plates is fitted with two

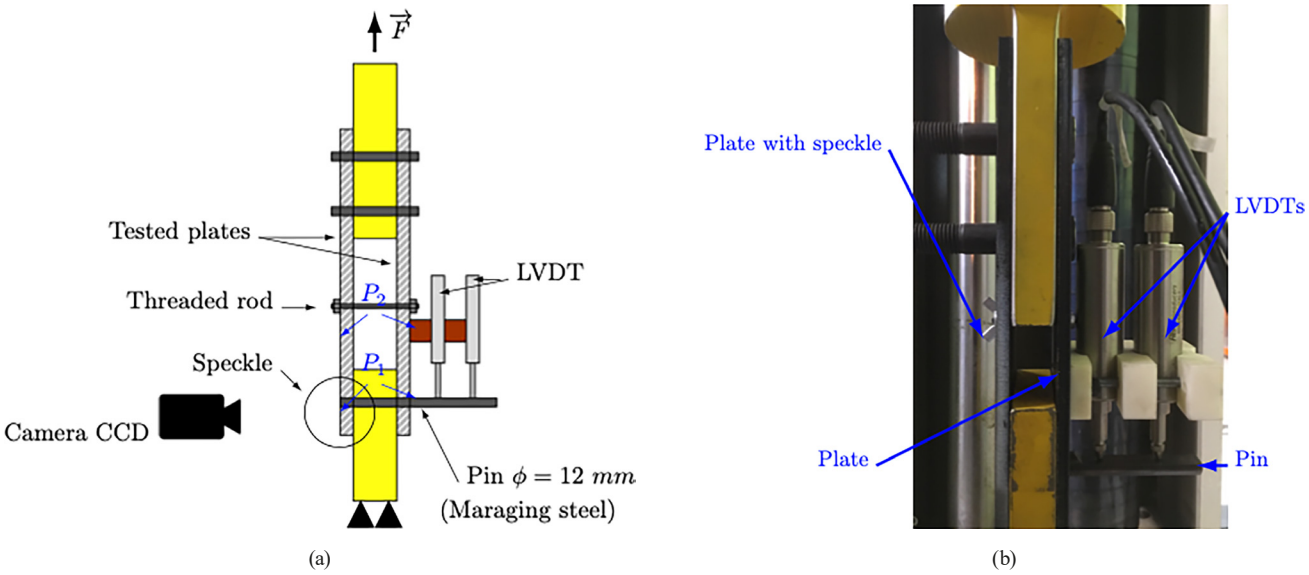

(a) (b)

Fig. 2 Experimental setup: (a) schematic view with displacement measurement positions (left: DIC; right: LVDT); (b) Side view of the experimental setup

LVDT sensors and the other plate is fitted with a DIC system. The LVDT sensors are used to obtain displacements mainly beyond the linear range of behavior. The DIC measurement used in the plate zone around the hole is mainly used in the initial phase, which is the aim of this study. The lower grip is fixed; the upper grip moves vertically. The load is transferred from the testing machine to the specimen by the upper yellow fixture, which is fixed on one side to the grip and on the other side to the two tested plates with two bolts. The displacement controlled tensile tests were carried out with a displacement rate of the crosshead machine chosen equal to 0.04 mm/s. In addition to the local measurement of the joint (LVDT and DIC), the load-displacement curves of the testing machine are also considered. The local measurements are carried out on one side of the fixture where the displacement is measured using two LVDT sensors and on the other side using the DIC technique.

During the test, the pin may bend due to the action of the plates on either side of the yellow fixture (Fig. 2). The use of the two LVDT sensors allows the tilt of the pin to be measured. It is shown that the maximum rotation is less than 2°. In the experimental test setup, the pin head was cut to allow the displacement of the surface under the pin to be measured. Consequently, a small diameter threaded dowel was used to limit the distance between the plates (Fig. 2). Out-of-plane displacement in the compression zone is not analyzed here because it occurs with large plastic deformations, largely beyond the nominally elastic phase on which the study focuses to determine the initial stiffness.

2.4 Full-field measurement technique

This section presents the image processing, from experimental acquisition to analysis of the results, which allows the relative displacement between the bolt and the plate to be obtained.

A PCO EDGE camera with a 14-bit 2048 × 2048-pixel CCD sensor and equipped with a 105 mm lens was used to capture images of the black and white speckle (Fig. 3 (b)) classically used for DIC. The speckle characteristics can affect the metrological performances of the technique, as detailed in [17]. For this reason, special attention was paid to the speckle deposition. The acquisition frequency of the camera is 0.43 image/s. During the tests, the surface was illuminated with a cold light source to obtain a quasi-uniform illumination of the speckles. Fig. 3 (a) gives an overview of the experimental setup. Images captured by the camera are then used to deduce displacement fields from the speckle images using an open source 2D Digital Image Correlation MATLAB program, Ncorr software [18]. The displacement fields obtained by DIC are well suited to measure the relative displacement between the plate and the bolt to characterize the load-displacement curve and the initial stiffness. The location of point $P2$ is chosen to correspond to the same location as the reference position of the LVDT transducers. This relative displacement is measured by the difference between the vertical displacement of points $P1$ and $P2$ (Fig. 3 (b)). Due to local crushing of the plate under the bolt, point $P1$ is located 0.5 mm below the contact point between the bolt and the plate hole as shown in Fig. 3 (b). The initial distance between point $P1$ and $P2$ is 65 mm.

(a) (b)

Fig. 3 Camera measurement setup: (a) overview of the experimental setup; (b) example of a speckle pattern near the zone of slotted hole with location of points *P*1 and *P*2 used to obtain the displacement between the bolt and the plate (*P*1: located 0.5 mm under the hole edge; *P*2: same location as LVDT transducer)

3 Experimental results and discussion

3.1 Load-displacement curves

This section compares the two displacement measurement techniques, DIC and LVDT. During the tensile tests, even if the pin material has high mechanical properties, it may bend, inducing additional displacement of the LVDT sensors as explained in Section 2.3. In addition, LVDT sensors can be sensitive to clearances in the connection and positioning of the sensors. This can create another source of overestimation of relative displacement.

By way of illustration, Fig. 4 (a) shows an example of the relative displacement u between points *P*1 and *P*2 (Fig. 3 (b)) obtained using the DIC technique and LVDT sensors. For each load level, the relative displacement u obtained by the DIC technique is smaller than that obtained by the LVDT sensors. This difference corresponds to the clearance in the internal part of the structure. DIC measurement avoids such measurement errors because it focuses on measuring the surface displacement of the specimens independently of the fixture. Consequently, the DIC technique is better suited to measuring displacement in the nominally elastic phase than the LVDT one. Therefore, in this study, the initial stiffness is calculated using the displacement obtained from the DIC measurement.

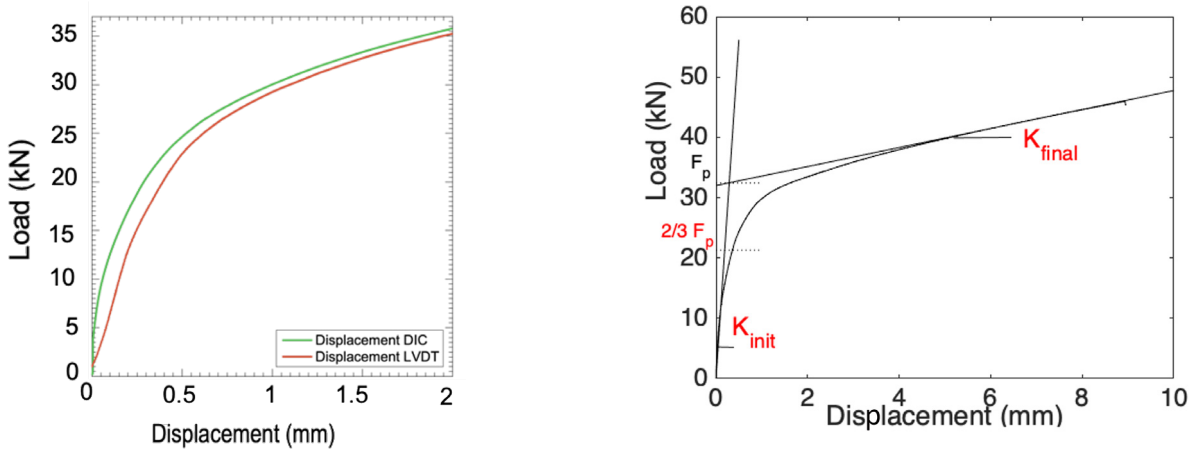

(a) (b)

Fig. 4 Example of load-displacement curves: (a) obtained using LVDT sensor or DIC; (b) bilinear behavior with the definition of plastic load, initial and final stiffnesses for specimen *E*2.5-1.75

A bi-linear behavior of the load-displacement curve can be observed in Fig. 4 (b). The determination of the slopes shown in this figure is based on the values of the time derivative of the load. The methodology is presented in detail in Section 3.2.1 for the initial slope. A similar method is used to determine the final slope. Further details can be found in [19].

The load-displacement curve shown in Fig. 4 (b) is a realistic representation of the mechanical behavior of slotted holes observed in [16, 20]. Thus, the first linear part, considered as the nominally elastic phase, is used to define the initial stiffness of the slotted holes in the bearing. For all specimens, the range of load values used to determine the initial stiffness in the nominally elastic phase remains below 2/3 of the plastic strength obtained from the experimental load-displacement curves, considering the intersection of the straight lines representing the initial stiffness and the tangent to the second part of the curve, as shown in Fig. 4 (b).

The global behavior and failure modes of plates with slotted holes depend on the length of the slot and the loaded end distance [20]. It combines local support, bending and shearing of the loaded part under the bolt. The next section is dedicated to the determination of the initial stiffness due to these three loading cases.

3.2 Initial stiffness

3.2.1 Determination of the initial stiffness

Determining the initial stiffness and therefore the nominal elastic phase is a key issue. In fact, the behavior is not elastic in the strict sense, as yielding occurs at small displacements and is related to the plastic deformation of the hole in the bearing and to the yielding of the steel plate due to bending, as previously described by the authors in \ci [20]. Wald et al. defined the nominal elastic phase as the part of the curve that remains below 2/3 of the plastic strength [16]. This definition has been adopted in the current European standard [10] to define the elastic range of joints or parts of joints. Thus, in this paper, the initial stiffness represents the mechanical behavior of the plate with the slotted hole up to the elastic load, which is defined as 2/3 of the plastic strength. The plastic strength F_p is defined for all specimens as shown in Fig. 4 (b). The same approach is used to define the initial stiffness and the post-elastic stiffness. The intersection of the two curves defines the experimental strength value [16].

However, to enrich the analysis of the experimental results, an operator-independent methodology is proposed. This data processing method is developed to propose a qualified approach to define the initial stiffness based on the slope observed experimentally. The first objective of the method is to define, by means of an objective criterion, the displacement values that can be used to calculate the slope of the initial phase. The technique is based on a linear regression of the load-displacement curve in the nominal elastic phase considered first, up to the inflection of the curve. The points selected for regression correspond to those with the highest derivative force values. Due to the constant image acquisition frequency of the camera, the time between two images is constant. For each image, the time derivative of the load is calculated. The area of interest of the time derivative load curve is around the maximum derivative value. An important aspect is to select enough points close to the maximum value to perform a linear regression of the load-displacement curve with a coefficient of determination R^2 close to 1. Thus, in a first step, all points with a derivative value higher than 50% of the maximum value of the curve are selected, then a linear regression is performed on these points to obtain the coefficient of determination (in the least square sense). In a second step, an algorithm selects points with an upload speed close to the maximum value until a determination factor of at least 0.995 is obtained. This method provides a repeatable linear regression in the nominal elastic phase of the load-displacement curve.

An example of the time derivative load-displacement curve is shown in Fig. 5. The corresponding load-displacement curve is also plotted with the couple load F_k-displacement u_k, where the linear curve intersects the experimental one, also shown in the figure. The method is

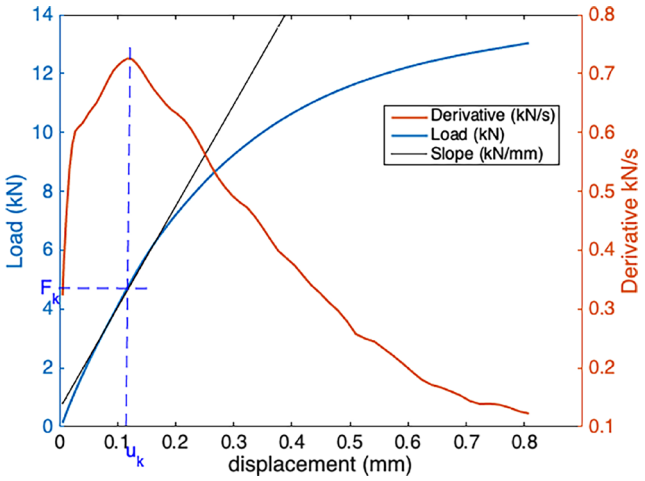

Fig. 5 Example of load-displacement curve and the corresponding temporal derivative load-displacement curve for specimen *E*1-1

used to obtain the experimental values of the initial stiffnesses for all the specimens tested. The results are presented in Section 4.

3.2.2 An analytical model for the initial stiffness

This section presents a model for determining the initial stiffness of the slotted hole joint. It is developed based on the observed competition between flexure and support of the end gap zone [20, 21].

Cavène et al. [20] have shown that the slot has two main behaviors: a flexible one characterized by a bending failure and a stiffer one characterized by a bearing failure. There are therefore two competing phenomena: the bearing and the bending of the end-distance zone in the nominally elastic phase. The stiffness must take these two components into account to predict the initial stiffness of the slotted cover plate.

The first component to be characterized is the bearing. Two models for predicting the bearing stiffness component are available in the literature. The first, proposed in Eurocode 3, is also used by Wald et al. [16].

The second model that defines stiffness in bearing was proposed by Rex and Easterling [14] for the \normal round hole. This model uses three components: one in bearing (see Eq. (1), one in bending and one in shearing, corresponding to a fixed end beam with a length equal to the diameter of the hole. The model based on experimental and numerical results is given in Eq. (1) for the bearing component:

$$K_{\text{bearing}} = 9 \times t \times f_y d^{0.8} \tag{1}$$

where f_y is the yield strength of the steel plate. The unit of the bolt diameter d is in mm. This model is used to define the initial or elastic stiffness component for the bearing. So, this formula is adapted for the initial zone, before 2/3 of the plastic strength.

The bending component corresponds to the flexibility of the end distance zone. The proposed model is based on Rex and Easterling's [14] for a normal round hole and is adapted here for a slotted hole. In the Rex and Easterling model, the bending stiffness is obtained for a fixed end beam and a single load at the center of the beam, which is well suited to a normal round hole. In the present case, with slotted holes, the bending stiffness is obtained for a simply supported beam with a length of $L_0 + d_0$ and an applied load at mid-span. The model is shown in Fig. 6.

A clamped beam model was also tested [19]. The average ratio between the initial stiffness obtained with the models and the experimental initial stiffness is equal to 1.03 for the clamped beam and 0.8 for the simply supported beam.

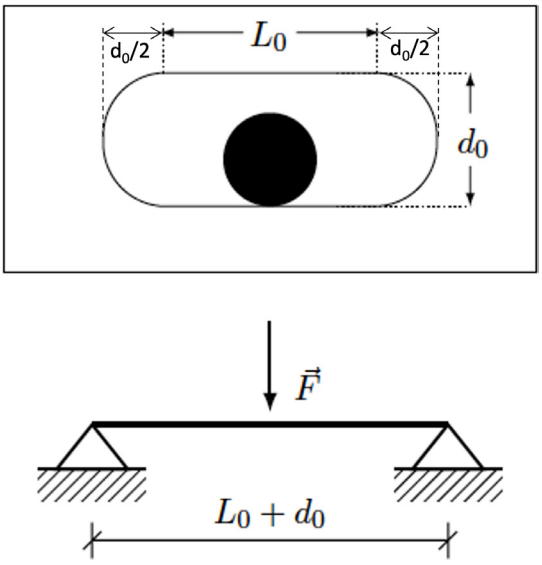

Fig. 6 Simply supported beam representing the end-distance bending model

However, the coefficient of determination R^2 of the linear curve representing the relationship between the stiffness values obtained by the model and the experiments is equal to 0.46 for the clamped beam and 0.86 for the simply supported beam. Therefore, a simply supported beam model was chosen to determine the initial stiffness. In fact, the real behavior can be considered as a semi-rigid restraint.

The bending component proposed by the authors is given in Eq. (2):

$$K_{\text{bending}} = \frac{48 \times E \times t \times \left(e_3 - \frac{d_0}{2}\right)^3}{12 \times \left(L_0 + d_0\right)^3} \tag{2}$$

where E is the elastic modulus of steel.

In addition, the slenderness of the end distance zone, namely the ratio $(L_0 + d_0)/(e_3 - d_0/2)$, varies from 1.33 for specimen E1-2 to 8 for specimen E3-1. Therefore, the shear contribution to stiffness must be considered. The shear stiffness component proposed by the authors is given in Eq. (3):

$$K_{\text{shearing}} = \frac{4 \times G \times t \times \left(e_3 - \frac{d_0}{2}\right)}{L_0 + d_0} \tag{3}$$

where G is the shear modulus of steel.

Based on the Rex and Easterling analysis, the final initial stiffness of the tested bolted joints depends on the association of the bending, shearing, and bearing components. In the present work, the three stiffness components are related in a similar way to obtain the equivalent model (Fig. 7). The corresponding stiffness is given in Eq. (4).

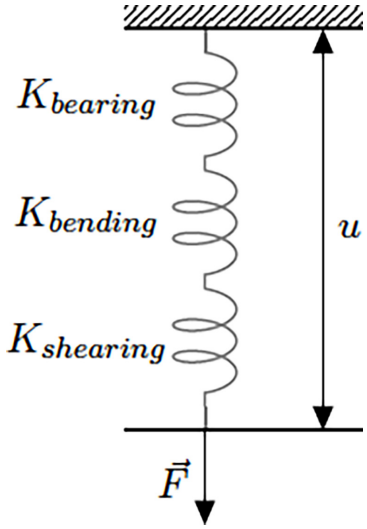

Fig. 7 Equivalent model of the end-distance stiffness

$$K_{\text{initial}} = \frac{1}{\frac{1}{9\times t\times f_y d^{0.8}} + \frac{12\times\left(L_0+d_0\right)^3}{48\times E\times t}\times\left(e_3-\frac{d_0}{2}\right)^3 + \frac{L_0+d_0}{4\times G\times t}\times\left(e_3-\frac{d_0}{2}\right)} \quad (4)$$

The results presented in Section 4.2 illustrate the contribution of each component (bearing, bending, and shearing) to the initial stiffness obtained from the tests, depending on the geometry of the specimens studied.

4 Experimental and analytical results

4.1 Experimental results

All images recorded during the tests allowed the determination of displacement fields in both horizontal and vertical directions using the DIC technique. An example of a vertical displacement field is shown in Fig. 8 for a load of 4 kN. The displacement values are symmetrical, showing the good alignment of the vertical load with respect to the joint. The maximum displacement can be seen just below the contact zone (red part of the figure below the slotted hole).

Fig. 9 shows the load-displacement curves obtained for all the tests. In these figures the displacements are obtained from LVDT sensors to show the full range of behavior of the joints tested. Each figure is plotted for the same end distance e_3. For comparisons, *E*0-*i* load-displacement curves are added Fig. 9, as control tests. They correspond to samples with circular hole.

All these curves are used to determine the initial stiffness using the methodology presented in Section 3.2.1. To illustrate the results, some examples of load-displacement curves with initial slope are shown in Fig. 10.

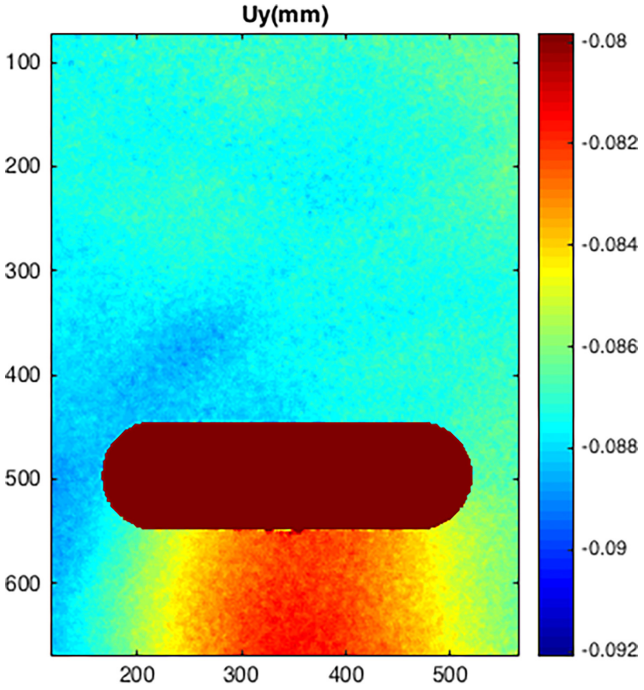

Fig. 8 Example of the vertical displacement field obtained for specimen *E*2.5-1.75 for a load value of 4 kN

Table 2 summarizes the average values of initial stiffness for each geometry of the specimens obtained by the approach presented in Section 3.2.1. To evaluate the variability of the results, the coefficient of variation (COV) is calculated for each geometry of the specimens tested. These results show a high variation around the mean.

The three columns in Table 2 give u_k, F_k and 2/3 F_P. The u_k and F_k correspond to the displacement and load values where the linear curve intersects the experimental one (Fig. 5). F_P corresponds to the plastic load determined by the method used in [16]. From the last two columns it can be concluded that F_k is less than 2/3 F_P, thus validating the procedure used to determine the initial stiffness of each tested joint.

The results show that there is significant variability between experimental stiffness values for the same geometry. The average experimental coefficient of variation is 12%. These results do not include results with inconsistent values.

4.2 Initial stiffness of the proposed model

In this section the initial stiffness of the proposed model defined by Eq. (4) is calculated. The results are presented in Table 3, showing the contribution of each component and the ratio between the model and the experimental initial stiffnesses. The average value of the ratio between the analytical stiffness obtained from Eq. (4) and the experimental one is calculated for all the specimens tested (model value/qualified approach value). It is equal to 0.80 with a COV equal to 30%.

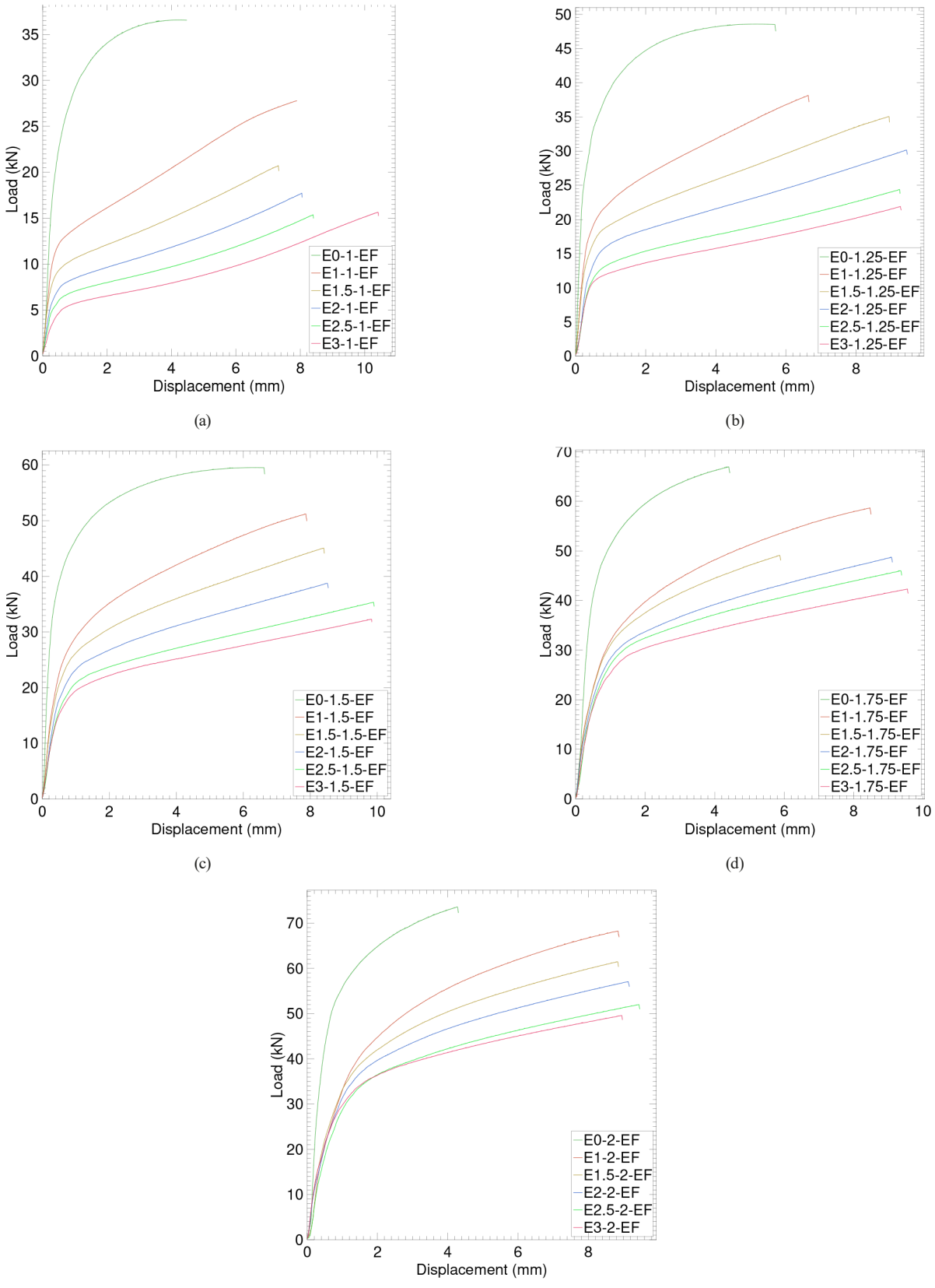

Fig. 9 Load-displacement curves for all specimens: (a) *Ei*-1 specimens, (b) *Ei*-1.25 specimens, (c) *Ei*-1.5 specimens, (d) *Ei*-1.75 specimens, (e) *Ei*-2 specimens, $i = 0$ (normal round hole) to 3 (see Table 1 for the notations of specimens)

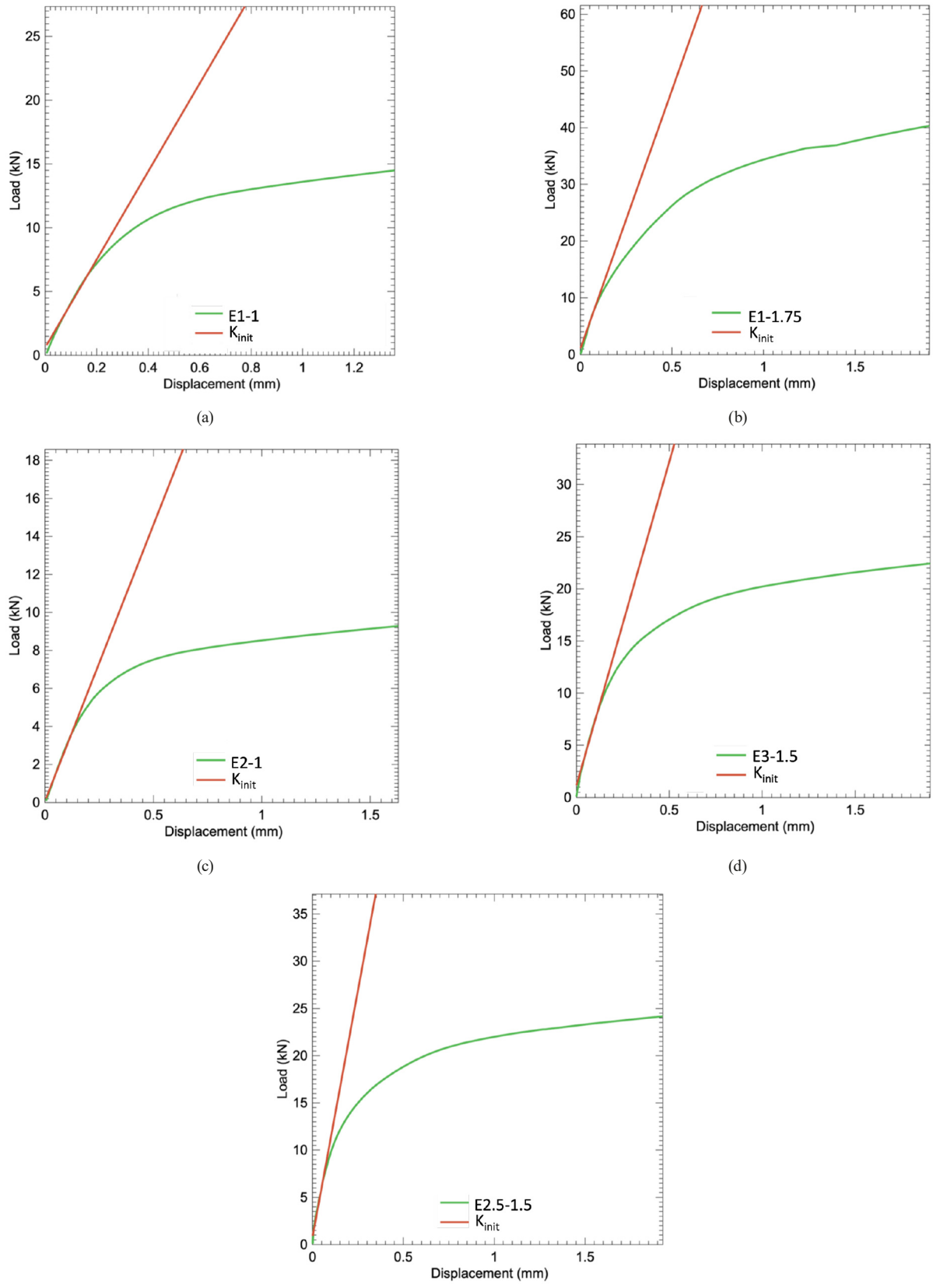

Fig. 10 Load-displacement curves for some specimens: (a) *E*1-1 specimen, (b) *E*1-1.75 specimen, (c) *E*2-1 specimen, (d) *E*3-1.5 specimen, (e) *E*2.5-1.5 specimens, (see Table 1 for the notations of specimens)

Table 2 Experimental values of initial stiffness (mean and coefficient of variation) with the limit of load (used in DIC technique) and the 2/3 F_P load

Specimen	$k_{initial}$		u_k	F_k	2/3 F_P
	mean (kN/mm)	COV (%)	(mm)	(kN)	(kN)
*E*0-1	136	24	0.04	11.0	21.2
*E*0-1.25	209	10.6	0.09	6.3	28.5
*E*0-1.5	287	1.0	0.03	12.9	34.3
*E*0-1.75	335	1.0	0.03	14.7	36.2
*E*0-2	389	3.6	0.02	13.0	30.1
*E*1-1	31	14.7	0.12	4.7	8.3
*E*1-1.25	97	4.0	0.05	7.1	15.0
*E*1-1.5	126	0.8	0.03	7.0	20.9
*E*1-1.75	102	14.5	0.07	7.1	26.2
*E*1-2	187	4.5	0.02	6.6	31.2
*E*1.5-1	37	10.7	0.08	3.5	6.1
*E*1.5-1.25	62	27.6	0.06	6.7	12.4
*E*1.5-1.5	116	0.4	0.04	7.2	18.5
*E*1.5-1.75	141	8.0	0.02	6.9	22.4
*E*1.5-2	161	8.6	0.02	7.6	26.9
*E*2-1	32	14.4	0.05	1.4	4.9
*E*2-1.25	48	3.2	0.13	6.2	10.5
*E*2-1.5	89	4.5	0.05	6.7	15.3
*E*2-1.75	118	3.3	0.04	6.1	22.1
*E*2-2	126	31.8	0.07	6.2	25.0
*E*2.5-1	28	23.2	0.04	1.5	3.9
*E*2.5-1.25	52	11.9	0.08	5.4	9.0
*E*2.5-1.5	90	22.4	0.05	6.2	14.8
*E*2.5-1.75	111	5.5	0.04	6.5	21.2
*E*2.5-2	143	14.7	0.04	6.9	23.4
*E*3-1	25	14.4	0.04	1.2	3.0
*E*3-1.25	51	4.9	0.10	6.0	7.9
*E*3-1.5	68	10.7	0.08	6.1	13.6
*E*3-1.75	107	3.1	0.05	7.5	18.9
*E*3-2	110	18.6	0.06	7.7	22.8

Table 3 Analytical stiffness of the proposed model with the contribution of each component and ratio model/exp

Specimen	$k_{initial}$	Contribution to the $k_{initial}$ (%)			ratio
	kN/mm	Bearing	Bending	Shearing	Model/exp
*E*0-1	114.09	70.15	18.12	11.73	0.84
*E*0-1.25	136.88	84.17	6.44	9.39	0.66
*E*0-1.5	145.73	89.61	2.90	7.49	0.51
*E*0-1.75	150.10	92.29	1.53	6.18	0.45
*E*0-2	152.65	93.87	0.89	5.24	0.39
*E*1-1	47.83	29.4	60.8	9.8	1.54
*E*1-1.25	88.63	54.5	33.3	12.2	0.91
*E*1-1.5	114.09	70.2/70.2	18.1	11.7	0.91
*E*1-1.75	128.45	79.0	10.4	10.6	1.26
*E*1-2	136.88	84.2	6.4	9.4	0.73
*E*1.5-1	29.83	18.3	74.0	7.7	0.81
*E*1.5-1.25	65.74	40.4	48.3	11.3	1.06
*E*1.5-1.5	94.92	58.4	29.4	12.2	0.82
*E*1.5-1.75	114.09	70.2	18.1	11.7	0.81
*E*1.5-2	126.18	77.6	11.6	10.8	0.78
*E*2-1	19.20	11.8	82.3	5.9	0.6
*E*2-1.25	47.83	29.4	60.7	9.8	1.0
*E*2-1.5	76.63	47.1	41.1	11.8	0.86
*E*2-1.75	98.75	60.7	27.1	12.2	0.84
*E*2-2	114.08	70.2	18.1	11.7	0.78
*E*2.5-1	12.85	7.9	87.5	4.6	0.46
*E*2.5-1.25	34.83	21.4	70.2	8.4	0.67
*E*2.5-1.5	60.77	37.4	51.7	10.9	0.67
*E*2.5-1.75	83.72	51.5	36.5	12.1	0.75
*E*2.5-2	101.32	62.3	25.5	12.2	0.71
*E*3-1	8.94	5.5	90.8	3.7	0.36
*E*3-1.25	25.65	15.8	77.2	7/0	0.50
*E*3-1.5	47.83	29.5	60.7	9.8	0.70
*E*3-1.75	69.95	43.0	45.5	11.5	0.65
*E*3-2	88.63	54.5	33.3	12.2	0.81

This last value is relatively high, especially for small end distances e_3 which are outside the EC3 recommendations. If these cases are excluded, the coefficient of variation drops to 16%, which is quite satisfactory. These results confirm that the predicted initial stiffness is acceptable in terms of the variability of the experimental results.

Moreover, the study of the contribution of each component shows that an increase in the end distance induces an increase in the contribution of the bearing component (see, for example, the red values for a hole length L_0 equal to the diameter d_0 in Table 3) and a decrease in the bending component (see, for example, the blue values for L_0 in Table 3. The shear component is less dependent on the geometry with a ratio of less than 0.12 which remains relatively constant for each hole length. However, a small increase in the contribution of the shear component can be observed as the end distance increases. Finally, for the same end distance, the bearing component naturally decreases as the hole length L_0 increases (see green values for example for 1.5 d_0 in Table 3).

4.3 Discussion

In this section the initial stiffnesses obtained experimentally and from the proposed model are analyzed. The results are shown in Figs. 11, 12. The main analysis concerns the evolution of the initial stiffness with the two geometric parameters: hole length L_0 and end-distance e_3.

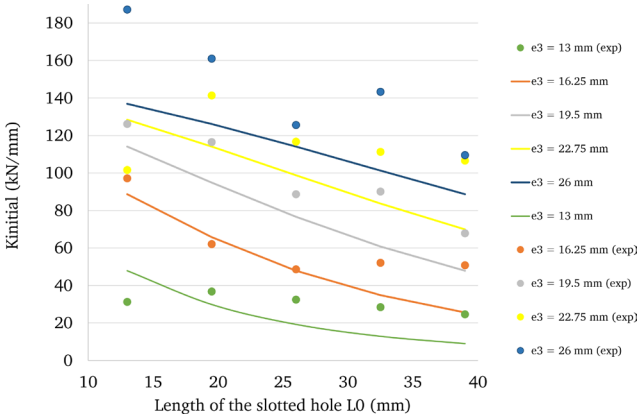

Fig. 11 Experimental (dots) and proposed model values (solid line) of the initial stiffness as a function of the length of the slotted hole

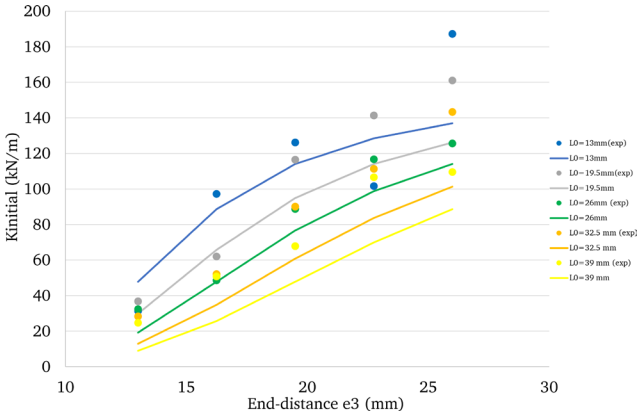

Fig. 12 Experimental (dots) and proposed model values (solid line) of the initial stiffness as a function of the slotted hole

The results presented in Fig. 11 clearly show that as the hole length L_0 increases, both the experimental and analytical initial stiffnesses decrease globally. Table 3 shows that the bending contribution increases with length L_0 and becomes dominant. Furthermore, as the bending component proposed in Eq. (2) is inversely proportional to the cubic length L_0, the analytical initial stiffness logically decreases. The analytical model generally underestimates the stiffness. It needs to be improved.

The evolution of the experimental values of the initial stiffness with the end distance values is shown in Fig. 12. Whatever the hole length L_0, the stiffness increases with the end distance, except for specimen *E*1-1.75.

5 Conclusions

The aim of this paper is to propose a new methodology for the determination of the initial stiffness of slotted cover plates. For this purpose, a large experimental campaign on 59 specimens with 25 different geometries has been presented to measure the initial stiffness of cover plates with slotted holes. The measurement of the displacement in the elastic phase was carried out using both LVDT sensors and the DIC technique. The study of the results has shown that the DIC technique is well suited to characterize the displacement representing the behavior of the slotted holes in the elastic phase, due to the independence of this measurement technique from the setup clearances and deformations. The analysis of the results shows that:

- for a fixed end-distance, the increase of the hole length induces a decrease of the stiffness.
- for a fixed hole length, the increase of the end-distance induces an increase of the stiffness.

From the experimental results, a new methodology has been proposed to determine the initial stiffness of slotted cover plates based on the maximum of the time derivative load. This methodology allows the same initial stiffness to be obtained regardless of the operator.

In addition, an analytical model has been proposed based on three stiffness components: one in bearing, one in bending and one in shearing. The proposed model appears to be in good overall agreement with the experimental results. The analysis of these results allows 2 main observations to be made regarding whether the slotted holes are short ($L_0 < 1.25d_0$) or long ($1.25d_0 < L_0 < 3.5d_0$):

- for short, slotted holes with an end distance $e_3 < 1.25d_0$, the bending component is dominant compared to the bearing component. For large end distances ($e_3 \geq 1.25d_0$), the bearing component is dominant.
- for long slots with small end distance $e_3 < 1.5d_0$: the bending component is dominant compared to the bearing component. For larger end distances ($e_3 \geq 1.5d_0$), the bearing component is dominant.
- finally, the shear component remains relatively constant for a given hole length.

A work in progress aims at modeling this connection with a bilinear law. The idea is to allow defining the stiffness in the plastic phase and the load corresponding to the transition between the elastic and the plastic phases.

Conflict of interest

The authors declare that they have no conflict of interest.

References

[1] Toussaint, E., Durif, S., Bouchaïr, A., Grédiac, M. "Strain measurements and analyses around the bolt holes of structural steel plate connections using full-field measurements", Engineering Structures, 131(15), pp. 148–162, 2017. https://doi.org/10.1016/j.engstruct.2016.11.033

[2] Tajeuna, T. A. D., Legeron, F., Labossière, P., Demers, M., Langlois, S. "Effect of geometrical parameters of aluminum-to-steel bolted connections", Engineering Structures, 102, pp. 344–357, 2015. https://doi.org/10.1016/j.engstruct.2015.08.010

[3] Može, P., Beg, D., Lopatič, J. "Net cross-section design resistance and local ductility of elements made of high strength steel", Journal of Constructional Steel Research, 63(11), pp. 1431–1441, 2007. https://doi.org/10.1016/j.jcsr.2007.01.009

[4] Može, P., Beg, D. "A complete study of bearing stress in single bolt connections", Journal of Constructional Steel Research, 95, pp. 126–140, 2014. https://doi.org/10.1016/j.jcsr.2013.12.002

[5] Rogers, C. A., Hancock, G. J. "Failure Modes of Bolted-Sheet-Steel Connections Loaded in Shear", Journal of Structural Engineering, 126(3), pp. 288–296, 2000. https://doi.org/10.1061/(ASCE)0733-9445(2000)126:3(288)

[6] Driver, R. G., Grondin, G. Y., Kulak, G. L. "Unified block shear equation for achieving consistent reliability", Journal of Constructional Steel Research, 62(3), pp. 210–222, 2006. https://doi.org/10.1016/j.jcsr.2005.06.002

[7] Huns, B. B. S., Grondin, G. Y., Driver, R. G. "Tension and shear block failure of bolted gusset plates", Canadian Journal of Civil Engineering, 33(4), pp. 395–408, 2006. https://doi.org/10.1139/l05-104

[8] Salih, E. L., Gardner, L., Nethercot, D. A. "Bearing failure in stainless steel bolted connections", Engineering Structures, 33(2), pp. 549–562, 2011. https://doi.org/10.1016/j.engstruct.2010.11.013

[9] Kim, T. S., Kuwamura, H., Cho, T. J. "A parametric study on ultimate strength of single shear bolted connections with curling", Thin-Walled Structures, 46(1), pp. 38–53, 2008. https://doi.org/10.1016/j.tws.2007.08.009

[10] AFNOR Editions "NF EN 1993-1-8 Eurocode 3: Design of steel structures - Part 1-8: Design of joints", AFNOR Editions, La Plaine Saint-Denis, France, 2005.

[11] Weynand, K., Jaspart, J.-P., Steenhuis, M. "The stiffness model of revised annex j of eurocode 3", In: Bjorhovde, R., Colson, A., Zandonini, R. (eds.) Connections in Steel Structures III, Pergamon, 1996, pp. 441–452. ISBN 978-0-08-042821-5 https://doi.org/10.1016/B978-008042821-5/50100-0

[12] Wuwer, W., Zamorowski, J., Swierczyna, S. "Lap joints stiffness according to Eurocode EC3 and experimental investigations results", Archives of Civil and Mechanical Engineering, 12(1), pp. 95–104, 2012. https://doi.org/10.1016/j.acme.2012.03.017

[13] Plumier, A. "Behaviour of connections", Journal of Constructional Steel Research, 29(1–3), pp. 95–119, 1994. https://doi.org/10.1016/0143-974X(94)90058-2

[14] Rex, C. O., Easterling, W. S. "Behavior and Modeling of a Bolt Bearing on a Single Plate", Journal of Structural Engineering, 129(6), pp. 792–800, 2003. https://doi.org/10.1061/(ASCE)0733-9445(2003)129:6(792)

[15] Araki, Y., Endo, T., Iwata, M. "Feasibility of improved slotted bolted connection for timber moment frames", Journal of Wood Science, 57(3), pp. 247–253, 2011. https://doi.org/10.1007/s10086-010-1165-7

[16] Wald, F., Sokol, Z., Moal, M., Mazura, V., Muzeau, J.-P. "Stiffness of cover plate connections with slotted holes", Journal of Constructional Steel Research, 60(3–5), pp. 621–634, 2004. https://doi.org/10.1016/S0143-974X(03)00133-0

[17] Bornert, M., Brémand, F., Doumalin, P., Dupré, J.-C., Fazzini, M., Grédiac, M., Hild, F., Mistou, S., Molimard, J., Orteu, J.-J., Robert, L., Surrel, Y., Vacher, P., Wattrisse, B. "Assessment of Digital Image Correlation Measurement Errors: Methodology and Results", Experimental Mechanics, 49(3), pp. 353–370, 2009. https://doi.org/10.1007/s11340-008-9204-7

[18] Blaber, J., Adair, B., Antoniou, A. "Ncorr: Open-Source 2D Digital Image Correlation Matlab Software", Experimental Mechanics, 55(6), pp. 1105–1122, 2015. https://doi.org/10.1007/s11340-015-0009-1

[19] Cavène, E. "Comportement des assemblages mixtes bois-métal avec trous oblongs" (Behavior of bolted timber-steel connections with slotted holes), PhD Thesis, Université Clermont Auvergne, 2019. [online] Available at: https://theses.hal.science/tel-02932933 (in French)

[20] Cavène, E., Durif, S., Bouchaïr, A., Toussaint, E. "Experimental study of slotted hole bolted cover-plate connection using full field measurement", Structures, 23, pp. 573–587, 2020. https://doi.org/10.1016/j.istruc.2019.09.003

[21] Cavène, E., Durif, S., Bouchaïr, A., Toussaint, E. "01.13: Experimental study of cover-plate bolted joints with large or slotted holes", ce/papers, 1(2–3), pp. 272–281, 2017. https://doi.org/10.1002/cepa.58